Visual Servoing of Cable-Driven Parallel Robots with Tension Management

Zane Zake[1,2], François Chaumette[3], Nicolò Pedemonte[2], and Stéphane Caro[1,4]

***Abstract*— Cable-driven parallel robots (CDPRs) are a type of parallel robots, where cables are used instead of rigid links. This leads to many advantages, such as large workspace, low mass in motion and simple reconfiguration. The drawbacks are accuracy issues and complex cable management. Indeed, it is usual that cables become slack. That can be caused by, for example, cable mass, uncertainties in the system, and a higher number of cables than the number of degrees of freedom of the moving-platform. This reduces CDPR stiffness and degree of actuation. While visual servoing provides good accuracy and is robust to different perturbations in the system and to modeling errors, it does not deal with cable slackness. Thus, a CDPR with visual servoing can become underactuated due to cable slack. We propose in this paper to enrich visual servoing with a tension correction algorithm. Experimental results show reduction of slackness and thus avoiding slackness-related trajectory perturbations and loss of stability.**

I. INTRODUCTION

Parallel robots have multiple kinematic chains connecting the end-effector, also known as the moving-platform (MP), and the base. In Cable-Driven Parallel Robots (CDPRs) the rigid links are replaced by cables. This change leads to many advantages, such as reduced mass in motion, large workspace, high payload capacity, and reconfigurability [1]. The drawbacks include unidirectional cable force. Indeed, a cable can only pull, yet it cannot push. Due to this, at least $m = n+1$ cables are needed to fully constrain n degrees of freedom (DoF) [2], making a CDPR redundant in actuation to degree $r = m-n$. Generally, eight cables are used for six DoF motion, because this increases the CDPR workspace [3]. In model-based approaches CDPR accuracy is directly tied to the choice of CDPR model. For instance, cable elasticity and pulley kinematics need to be taken into account to ensure acceptable accuracy [4, 5].

There are multiple ways to use a vision system for controlling CDPRs. A straightforward way is to use a camera mounted on the base to retrieve the MP pose [6]–[9], which avoids the need of the Direct Kinematic Model (DKM). For CDPRs with a large workspace, multiple cameras are usually required, e.g. three cameras in [7], four cameras in [6] and six infrared cameras in [8]. When the goal is to improve the robot accuracy with respect to a target, a camera is usually mounted on the MP [10]–[12]. Thus, both the camera and the MP approach the target simultaneously. In that case, the MP is not observed, but its pose is required in the control scheme. For instance, the DKM was used in [10] to retrieve the MP pose of a simplified spatial CDPR with three translational DoF. On the contrary, in [11] and [12] the use of DKM was avoided by coarsely estimating the MP pose. Indeed, it is possible to estimate the current MP pose, given the previous pose, the robot velocity sent to the low-level controller and the time interval, assuming that the very first initial pose is known. While visual servoing (VS) of a CDPR is very robust to many kinds of perturbations [11, 12] and remains accurate with respect to (wrt) the target, the cables tend to become slack. Furthermore, a vicious circle can be observed. As cables become slack, they do not produce the desired MP motion. Therefore, the error in the MP pose estimation increases. The worse the MP pose estimation, the slacker the cables. Conversely, the slacker the cables, the worse the MP pose estimation. This is also true for the cable length-based DKM computation for a simplified CDPR model as in [10].

Cable slackness is not specific to VS of CDPRs with a camera embedded on their MP. On the contrary, it is a common problem, which usually occurs over time due to discrepancies between the CDPR and its model. For example, a control technique that relies on a good knowledge of initial MP pose and then controls the robot via motor position commands is subject to cable slackness. In [13] the cable lengths are computed for a desired MP pose of a fully-constrained CDPR. To avoid cable slackness and to improve robot stiffness, a complex cable length adjustment based on current tension sensor measurements and the output of a tension distribution algorithm (TDA) is implemented. The TDA can also be used in tension or torque control of a fully-constrained CDPR [14, 15], thus ensuring that tensions in cables correspond to the desired MP pose. Even with an external measurement of the MP pose, cable slackness can occur, if the model does not correspond to the real CDPR, thus often complex cable models are used [4, 6].

The goal of this paper is to propose a simple algorithm that deals with cable slackness. Unlike the mentioned approaches, the proposed algorithm does not rely on the knowledge of the MP pose, the use of a TDA, nor a complex cable modeling depending on cable angles perceived by cameras [6].

For a redundantly actuated CDPR, having r cables slack does not prevent the MP from remaining in a given pose in static configuration. However, no matter the control ap-

This work is supported by IRT Jules Verne (French Institute in Research and Technology in Advanced Manufacturing Technologies for Composite, Metallic and Hybrid Structures) in the framework of the PERFORM project.

[1]Laboratoire des Sciences du Numérique de Nantes, UMR CNRS 6004, 1, rue de la Noë, 44321 Nantes, France, Zane.Zake@ls2n.fr

[2]IRT Jules Verne, Chemin du Chaffault, 44340, Bouguenais, France, nicolo.pedemonte@irt-jules-verne.fr

[3]Inria, Univ Rennes, CNRS, IRISA, Rennes, France, Francois.Chaumette@inria.fr

[4]Centre National de la Recherche Scientifique (CNRS), 1, rue de la Noë, 44321 Nantes, France, stephane.caro@ls2n.fr

TABLE I

NOTATION USED THROUGHOUT THE PAPER

- $\mathcal{F}_b$, $\mathcal{F}_p$, $\mathcal{F}_c$, $\mathcal{F}_o$ denote the base, MP, camera and object frames respectively (resp.).
- ${}^i\mathbf{T}_j = \begin{bmatrix} {}^i\mathbf{R}_j & {}^i\mathbf{t}_j \\ \mathbf{0} & 1 \end{bmatrix}$ is the transformation matrix from $\mathcal{F}_i$ to $\mathcal{F}_j$, where ${}^i\mathbf{R}_j$ and ${}^i\mathbf{t}_j$ are the rotation matrix and translation vector, resp.
- $\mathbf{A}^{-1}$ and $\mathbf{A}^\dagger$ are the inverse and the pseudo-inverse of $\mathbf{A}$, resp.
- $\widehat{\mathbf{A}}$ and $\hat{\mathbf{e}}$ are the estimations of $\mathbf{A}$ and $\mathbf{e}$, resp.
- $\mathbf{s}^*$ is the desired value of $\mathbf{s}$.
- $[\mathbf{e}]_\times$ denotes the cross-product matrix of vector $\mathbf{e}$.
- ${}^i\mathbf{a}$ is the vector $\mathbf{a}$ expressed in $\mathcal{F}_i$
- A_i and B_i are the exit and the anchor points of the ith cable, resp.

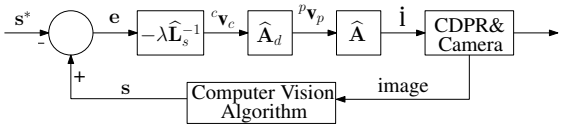

Fig. 1. Control scheme for visual servoing of a CDPR

proach, cable slackness leads to the CDPR being only partly responsive to the control output and thus not behaving as expected. Moreover, along a trajectory, cable slack will be transferred to different cables during the transition between two six-cable configurations [16], the MP becoming locally underactuated.

Thus, it is important to avoid cable slackness in order to improve the CDPR behavior and to keep it as stiff as possible. A tension correction algorithm is proposed in this paper to enrich VS control. Lyapunov stability analysis is used to evaluate the effect of cable slackness on the system.

The paper is organized as follows. Notations used in this paper are shown in Table I. VS of CDPRs is recalled in Section II. Tension correction is presented in Section III. Section IV contains the experimental validation and stability analysis. Finally, conclusions are drawn in Section V.

II. VISUAL SERVOING OF A CDPR

The VS control scheme of a CDPR is shown in Fig. 1. At every iteration of the control scheme an image is received from the onboard camera and it is sent to a computer vision algorithm, which outputs the current value of the feature vector $\mathbf{s}$. The nature of $\mathbf{s}$ is a function of the chosen VS approach. For example, it can simply be the target pose expressed in the camera frame $\mathcal{F}_c$ when a Pose-Based Visual Servoing (PBVS) is implemented [17]. In a more efficient VS approach, named 2½D visual servoing (2½D VS), the feature vector $\mathbf{s}$ contains both 2D and 3D features. For example, if $\mathbf{s} = [{}^{c^*}\mathbf{t}_c^T \;\; x_o \;\; y_o \;\; \theta u_z]^T$ [18, 19], then, both the target center-point trajectory in the image and the camera trajectory in the base frame $\mathcal{F}_b$ will be straight lines. This of course will be true if the system is well modeled. Here, ${}^{c^*}\mathbf{t}_c$ is the translation vector between $\mathcal{F}_c$ and $\mathcal{F}_{c^*}$; x_o and y_o are the image coordinates of target center-point $\mathbf{o}$; θu_z is the third component of axis-angle $\theta\mathbf{u}$ which corresponds to the rotation matrix ${}^{c^*}\mathbf{R}_c$ between $\mathcal{F}_{c^*}$ and $\mathcal{F}_c$. In this paper 2½D VS is used as in [12].

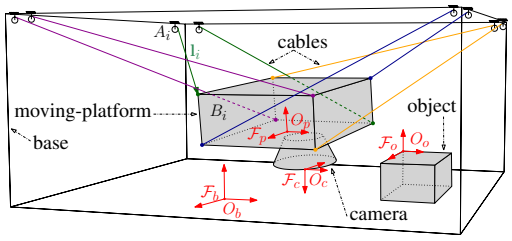

Fig. 2. Schematic of a CDPR with a camera mounted on its MP

The feature vector $\mathbf{s}$ is compared to the desired feature vector $\mathbf{s}^*$ to compute the error $\mathbf{e}$. To decrease the error $\mathbf{e}$, an exponential decoupled form is selected

$$\dot{\mathbf{e}} = -\lambda\mathbf{e} \tag{1}$$

where λ is a positive gain.

Camera velocity is then expressed as:

$${}^c\mathbf{v}_c = -\lambda\,\widehat{\mathbf{L}}_\mathbf{s}^{-1}\,\mathbf{e} \tag{2}$$

where $\mathbf{L_s}$ is the interaction matrix, defined such that $\dot{\mathbf{s}} = \mathbf{L_s}\,{}^c\mathbf{v}_c$, and its expression for 2½D VS is given in [18].

The MP twist, expressed in $\mathcal{F}_p$, is defined from the camera velocity ${}^c\mathbf{v}_c$ as follows:

$${}^p\mathbf{v}_p = \widehat{\mathbf{A}}_d\,{}^c\mathbf{v}_c \tag{3}$$

where $\widehat{\mathbf{A}}_d$ is the estimation of the adjoint matrix $\mathbf{A}_d$ [20]:

$$\mathbf{A}_d = \begin{bmatrix} {}^p\mathbf{R}_c & [{}^p\mathbf{t}_c]_\times\,{}^p\mathbf{R}_c \\ \mathbf{0}_3 & {}^p\mathbf{R}_c \end{bmatrix} \tag{4}$$

The Forward Jacobian matrix $\mathbf{A}$ of the manipulator relates the cable velocity vector i̇ to the MP twist ${}^p\mathbf{v}_p$:

$$\dot{\mathbf{l}} = \widehat{\mathbf{A}}\,{}^p\mathbf{v}_p \tag{5}$$

Fig. 2 illustrates the main components of a CDPR and the frames of interest. For the modeling, the cables are supposed to be non-elastic and massless. The pulleys are assumed to be small, thus their radius is neglected. The components of matrix $\mathbf{A}$ can then be expressed in the MP frame $\mathcal{F}_p$ as [21]:

$$\mathbf{A} = \begin{bmatrix} {}^p\mathbf{u}_1^T & ({}^p\mathbf{b}_1 \times {}^p\mathbf{u}_1)^T \\ \vdots & \vdots \\ {}^p\mathbf{u}_m^T & ({}^p\mathbf{b}_m \times {}^p\mathbf{u}_m)^T \end{bmatrix} \tag{6}$$

where ${}^p\mathbf{u}_i$ is the unit vector of ${}^p\overrightarrow{A_iB_i}$, pointing from the exit point A_i to the anchor point B_i of the ith cable, and ${}^p\mathbf{b}_i$ is the vector pointing from the origin of MP frame $\mathcal{F}_P$ to B_i.

Vector ${}^p\mathbf{u}_i$ is known from the MP pose estimation in the base frame $\mathcal{F}_b$. As recalled in the introduction and described in [11, 12], it is indeed possible to coarsely estimate the MP pose by successive integration of the control output.

The model of the system shown in Fig. 1 is written by injecting Eqs. (2), (3) and (5) into (1):

$$\dot{\mathbf{e}} = \mathbf{L_s}\,\mathbf{A}_d^{-1}\mathbf{A}^\dagger\,\dot{\mathbf{l}} \tag{7}$$

The output of the control scheme, that is, the cable velocity vector l̇, is expressed by injecting (2) and (3) into (5):

$$\dot{\mathbf{l}} = -\lambda\,\widehat{\mathbf{A}}\,\widehat{\mathbf{A}}_d\,\widehat{\mathbf{L}}_\mathbf{s}^{-1}\,\mathbf{e} \tag{8}$$

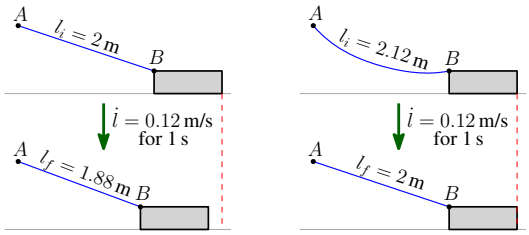

Fig. 3. Effect of cable slackness on MP displacement

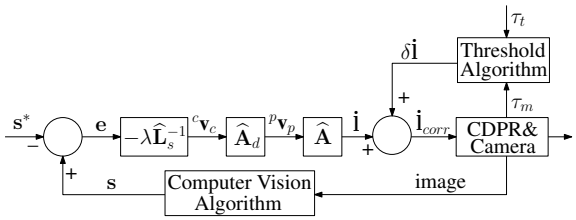

Fig. 4. Visual servoing control of a CDPR with a TCA

The closed-loop equation of the system is expressed by injecting (8) into (7):

$$\dot{\mathbf{e}} = -\lambda\,\mathbf{L_s}\,\mathbf{A}_d^{-1}\,\mathbf{A}^{\dagger}\,\widehat{\mathbf{A}}\,\widehat{\mathbf{A}}_d\,\widehat{\mathbf{L}}_{\mathbf{s}}^{-1}\,\mathbf{e} \tag{9}$$

According to Lyapunov stability analysis [22], the stability criterion $\mathbf{\Pi}$ is defined as:

$$\mathbf{\Pi} = \mathbf{L_s}\,\mathbf{A}_d^{-1}\,\mathbf{A}^{\dagger}\,\widehat{\mathbf{A}}\,\widehat{\mathbf{A}}_d\,\widehat{\mathbf{L}}_{\mathbf{s}}^{-1} \tag{10}$$

For the system to be stable, $\mathbf{\Pi} > \mathbf{0}$ is a sufficient condition. Indeed, as long as this condition is fulfilled, it is clear from (9) that the error $\mathbf{e}$ will converge to $\mathbf{0}$.

III. Tension Correction

Due to modeling errors and the estimation of the MP pose, the cables can become slack during task execution. While some limited slackness does not make the system unstable, it acts as an additional perturbation. Indeed, if a cable is slack, applying a velocity to it will not produce the desired displacement of the MP. An example is shown in Fig. 3. Here, on the left a cable is in tension with initial length $l_i = 2\,\mathrm{m}$ and after applying a velocity $\dot{l} = 0.12\,\mathrm{m/s}$ for $1\,\mathrm{s}$ the final cable length is $l_f = 1.88\,\mathrm{m}$ and the MP has been moved. On the right the initial location of points A and B is the same as before, but the cable is now slack and its initial length is $l_i = 2.12\,\mathrm{m}$. With the same cable velocity, the final cable length becomes $l_f = 2\,\mathrm{m}$, but the MP has not moved.

Since with slack cables the actual displacement of the MP differs from the estimated one, the MP pose estimation accumulates additional errors. This in turn leads to computation of cable velocities that may increase cable slackness.

Cable slackness can be detected in several ways. A set of four stereo-cameras is used in [6] to determine the cable angle, which in combination with MP pose measurement allowed the system to detect cable slackness. Kraus *et al.* in [13] used tension sensors to directly measure cable tensions. The measurements were then compared to the output of a TDA and a cable length correction was produced. The final control output was a sum of the inverse kinematics output and the correction. From their experiments, all the cables of a fully-constrained CDPR are in tension and the cable tensions have tripled after correction. As a consequence, the stiffness of the manipulator is substantially increased.

Unlike [13] where a position control scheme is developed, our control is in velocity. Thus, it is necessary to relate the cable tension measurements with cable velocities. To do this we propose the control scheme shown in Fig. 4.

Here, at every iteration cable tensions are measured and recorded in vector $\boldsymbol{\tau}_m$. Each component of this vector is then compared to a threshold tension τ_t and the ith component $\delta\dot{l}_i$ of the cable velocity correction vector $\delta\dot{\mathbf{l}}$ is computed as:

$$\delta\dot{l}_i = \begin{cases} -k_c(\tau_t - \tau_{m_i}) \text{ if } \tau_{m_i} < \tau_t, \quad i = 1, \ldots, m \\ 0 \text{ otherwise} \end{cases} \tag{11}$$

where τ_{m_i} is the measured tension of the ith cable, and k_c is a positive gain that needs to be tuned. The tension τ_t is the value under which the cable is considered to be slack.

The resulting behavior depends on the sign of ith cable velocity $\dot{l}_i$ computed by the controller. Note that negative velocity leads to the cable becoming shorter, and positive velocity leads to the cable becoming longer. Furthermore, according to (11) $\delta\dot{l}_i$ is not positive. Thus applying $\delta\dot{l}_i$ to a negative $\dot{l}_i$ results in cable length reducing faster. Applying $\delta\dot{l}_i$ to a positive $\dot{l}_i$ results in cable length increasing slower.

It should be noted that the correction speed is a function of the gain k_c. The greater the gain, the faster the correction. However, setting k_c too high may perturb the main controller. Thus, k_c should be tuned based on the frequency of the TCA loop. Furthermore, k_c is used to change the order of magnitude between the tension difference and cable velocities. For example, if $(\tau_t - \tau_{m_i}) \approx 1\,\mathrm{N}$ and $\dot{l}_i \approx 0.05 = 5 \times 10^{-2}\,\mathrm{m/s}$, then k_c will be defined as $k_c = 10^{-2}\,\mathrm{m/Ns}$.

The threshold τ_t is a tension that is feasible for every cable no matter the MP pose. Such a tension can be found by tracing a workspace, e.g. the Static Feasible Workspace (SFW) with ARACHNIS software [23], and choosing the lower tension bound τ_{lb}. Indeed, τ_{lb} is feasible for every cable and for all MP poses within SFW, thus it is a good pick for τ_t.

The proposed tension correction algorithm (TCA) is greatly simplified when compared to [13], while the overall control is more robust thanks to the use of VS. Indeed, instead of using a TDA and a complex computation of the final tension correction, we simply compare the current tensions to a threshold. In this case, the need for the knowledge of the MP pose is avoided since the tension threshold is constant. It is very convenient, because we only have a coarse MP pose estimation. Furthermore, using a coarse MP pose estimation with a TDA could be impossible. More precisely, the tension set provided by the TDA could be unattainable with the current MP pose in case of estimation errors. This would lead to perturbing the VS controller and possibly even making it unstable, thus failing the task. In addition, the simpler the calculations, the faster the controller response to each incoming image and tension measurement.

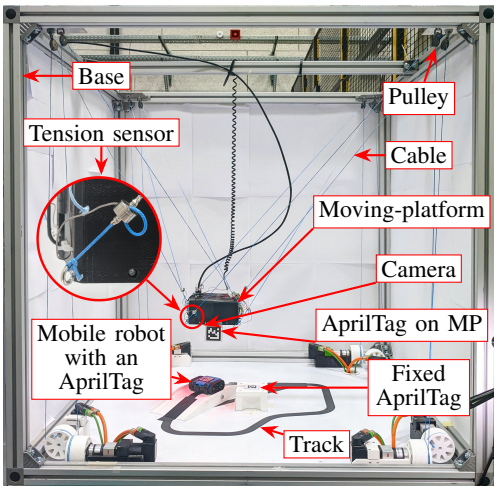

Fig. 5. ACROBOT: a CDPR prototype located at IRT Jules Verne, Nantes

The chosen expression of the CDPR model and thus stability criterion $\mathbf{\Pi}$ does not contain cable tensions. For CDPRs with light cables, if one cable becomes slack, as detected by tension measurements, then it will be considered non-existent. Indeed, a light cable exerts a negligible force on the MP when slack. Furthermore, while a cable is slack, reducing its length does not induce any MP motion. For the stability analysis the expression of the Jacobian matrix $\mathbf{A}$ is updated at every iteration accordingly. For example, if at $t = 0\,\text{s}$ tension $\tau_{m_1} < \tau_t$, then the corresponding row of matrix $\mathbf{A}$ is removed and it becomes a (7×6)–matrix. Furthermore, if more than two cables are slack, the Jacobian $\mathbf{A}$ will be rank deficient and the robot will be underactuated. Considering the stability criterion $\mathbf{\Pi}$, it is clear that once $\text{rank}(\mathbf{A}) < 6$, then $\text{rank}(\mathbf{\Pi}) < 6$ and thus the stability criterion will not be fulfilled, as shown in Section IV-C.

IV. Experimental Validation

A. Experimental Setup

A six-DoF suspended CDPR prototype with eight cables, named ACROBOT and shown in Fig. 5, is used to validate experimentally the effect of cable slackness on the system behavior. Its frame is a $1.2\,\text{m} \times 1.2\,\text{m} \times 1.2\,\text{m}$ cube. The MP size is $0.18\,\text{m} \times 0.17\,\text{m} \times 0.07\,\text{m}$ and its mass is 3.5 kg. The cables are Dyneema SK78 $\varnothing 2\,\text{mm}$. Tension sensors are mounted on the cables close to their anchor points B_i. They are calibrated for a range from -25 N to 75 N, with an accuracy of 0.24 N and repeatability of 0.01 N.

A camera is mounted on the MP facing the ground. The image resolution is set to 640×480 pixels. The camera observes one AprilTag [24], a fiducial marker that is used as a target, and algorithms from the ViSP library [25] recognize and localize it once it becomes visible in the image. From these measurements, the feature vector $\mathbf{s}$ is computed and compared to the desired feature vector $\mathbf{s}^*$, and the robot is controlled using (8) to reduce this difference.

The main loop frequency is 25 Hz. The TCA loop can be as fast as 512 Hz, but for the following experiments it was kept at 25 Hz. The tuning of gain λ for 2½D VS on ACROBOT is detailed in [12]. By tracing SFW with ARACHNIS [23], it was found that setting the lower bound tension $\tau_{lb} = 1\,\text{N}$ ensures that all cables are in tension, while keeping the workspace large. Thus, we set $\tau_t = \tau_{lb} = 1\,N$. Finally, TCA gain k_c is tuned to be 0.04 m/Ns.

B. Experiments with cable slackness at initial MP pose

For the first set of experiments, a fixed AprilTag, shown in Fig. 5, is observed by the onboard camera. The initial values are the following:

- ${}^b\mathbf{p}_{p_0} = \left[0.202\,m;\ 0.118\,m;\ 0.268\,m;\ -18°;\ 10°;\ 4°\right]$
- ${}^c\mathbf{p}_{o_0} = \left[0.1\,m;\ -0.05\,m;\ 0.26\,m;\ 165°;\ 10°;\ 179°\right]$
- $\mathbf{o}_0 = \left[0.38\,m;\ -0.19\,m\right]$

and desired values are selected to be:

- ${}^b\mathbf{p}_p^* = \left[-0.11\,m;\ -0.20\,m;\ 0.366\,m;\ 13°;\ -20°;\ 33°\right]$
- ${}^c\mathbf{p}_o^* = \left[-0.14\,m;\ 0.115\,m;\ 0.35\,m;\ 178°;\ -20°;\ 147°\right]$
- $\mathbf{o}^* = \left[-0.39\,m;\ 0.33\,m\right]$

where ${}^b\mathbf{p}_p$ is the MP pose in $\mathcal{F}_b$; ${}^c\mathbf{p}_o$ is the AprilTag pose in $\mathcal{F}_c$; and $\mathbf{o}$ stands for the AprilTag center-point coordinates in the image. The angles in pose parameters are Euler angles. Note that ${}^c\mathbf{p}_{o_i}$ and $\mathbf{o}_i$ are measured at every iteration i to be used in the control scheme. Meanwhile, ${}^b\mathbf{p}_{p_0}$ and ${}^b\mathbf{p}_p^*$ have been obtained from an external camera observing another AprilTag mounted on the MP, shown in Fig. 5, and serve as ground truth. It is different from the ${}^b\mathbf{p}_p$ used in the control.

Every experiment starts at the initial MP pose ${}^b\mathbf{p}_{p_0}$ corresponding to the initial feature vector $\mathbf{s}$. Similarly, the desired MP pose ${}^b\mathbf{p}_p^*$, corresponding to the desired feature vector $\mathbf{s}^*$, is the same for all experiments.

According to [16] only six cables need to be in tension to achieve any given pose with a suspended CDPR. Given our initial MP pose ${}^b\mathbf{p}_{p_0}$, slack can be introduced on l_1 and l_2. Once the MP was in its initial pose ${}^b\mathbf{p}_{p_0}$, the winches of cables $\mathcal{C}_1$ and $\mathcal{C}_2$ were turned to increase their length by 4 cm or 8 cm. Six experiments, named E_1 to E_6, are defined:

- E_1 is 2½D VS without cable slack;
- E_2 is 2½D VS with TCA without cable slack;
- E_3 is 2½D VS with 4 cm cable slack;
- E_4 is 2½D VS with TCA with 4 cm cable slack;
- E_5 is 2½D VS with 8 cm cable slack;
- E_6 is 2½D VS with TCA with 8 cm cable slack.

The experimental results are shown in Figs. 6 and 7. Please also refer to the attached video to see the recorded experiments. Cable lengths, velocities, and tensions for cables $\mathcal{C}_1$, $\mathcal{C}_2$, $\mathcal{C}_5$ and $\mathcal{C}_6$ are shown in Fig. 6. The curves for cables $\mathcal{C}_3$, $\mathcal{C}_4$, $\mathcal{C}_7$ and $\mathcal{C}_8$ are not shown. Due to the symmetry in CDPR design and the diagonal MP trajectory, they do not contain any significant information. The added slack can be seen in Figs. 6a and 6b, where cable lengths l_1 and l_2 are shown.

First, the behavior of the CDPR under 2½D VS control with slack and no TCA is analyzed. Cables $\mathcal{C}_1$ and $\mathcal{C}_2$ remain longer in E_3 and E_5 than in E_1 along most of the trajectory (gray and green curves against blue curve, resp., in Figs. 6a and 6b). Note that by the end of the trajectory the slack has been transferred to cables $\mathcal{C}_5$ and $\mathcal{C}_6$, as

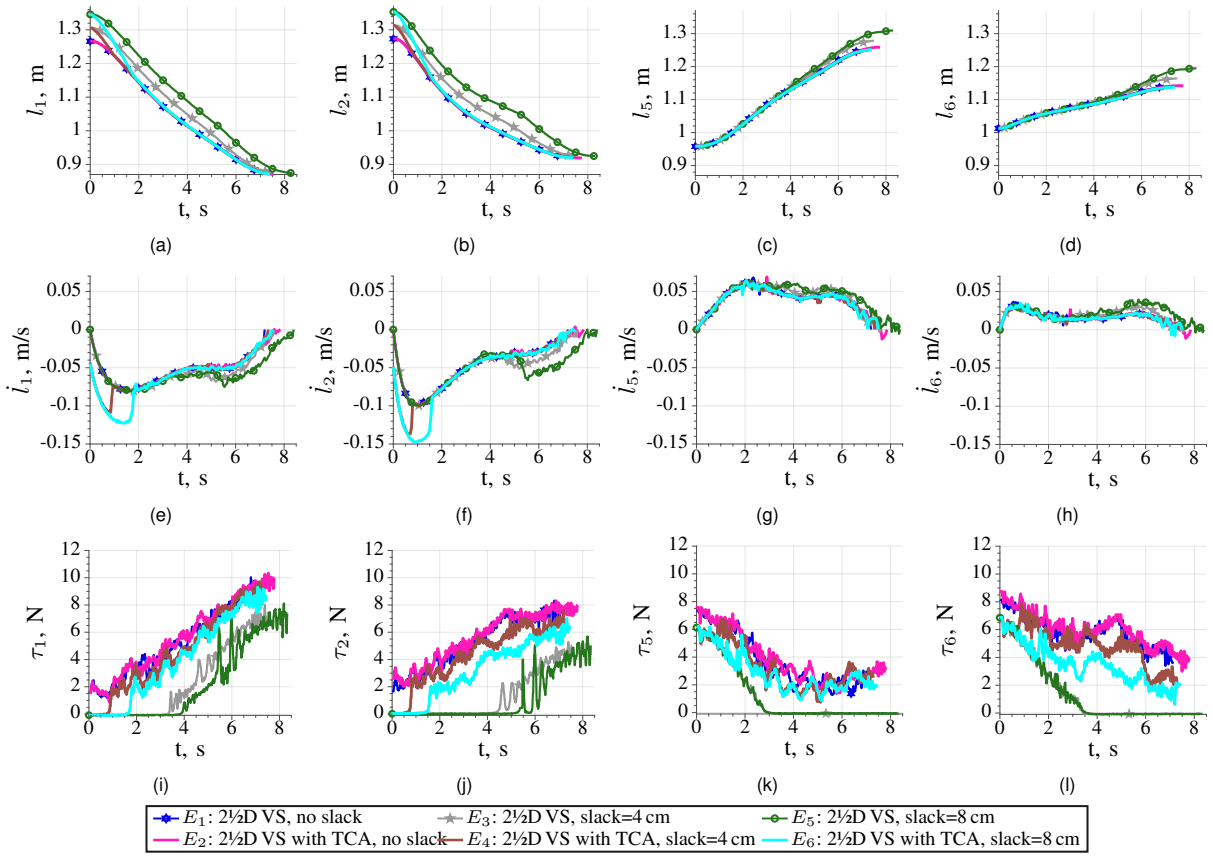

Fig. 6. Cable lengths l_i, cable velocities $\dot{l}_i$ and cable tensions τ_i for cables $\mathcal{C}_1$, $\mathcal{C}_2$, $\mathcal{C}_5$ and $\mathcal{C}_6$ on first, second and third rows, respectively

shown in Figs. 6c and 6d. Indeed, the six-cable configuration corresponding to the final MP pose is different from the initial one. The transfer of slack can also be seen in the tension measurements. Here, at first τ_1 and τ_2 are below the threshold, but by the end of the trajectory their values increase, while τ_5 and τ_6 decrease below τ_t. Note that more than two cables can become slack. For instance, at $t = 4\,\text{s}$ for both the gray and green curves, the cable tensions τ_2, τ_5 and τ_6 are below τ_t.

Once TCA is added to the controller, the behavior is different. It can be seen that the brown curve of E_4 aligns with the blue curve at approximately $t = 0.8\,\text{s}$ in Figs. 6a and 6b. Thus, at $t = 0.8\,\text{s}$ cable lengths l_1 and l_2 are equal for blue and brown curves of E_2 and E_4, resp. This is because up until $t = 0.8\,\text{s}$ velocities $\dot{l}_1$ and $\dot{l}_2$ were increased by the TCA velocity correction, as shown in Figs. 6e and 6f. Furthermore, at $t = 0.8\,\text{s}$ cable tensions τ_1 and τ_2 start to increase. Thus, at this moment cables are no longer slack. In E_6, shown in cyan, the correction of 8 cm slack takes about twice the time. Velocities $\dot{l}_1$ and $\dot{l}_2$ are increased until approximately $t = 1.5\,\text{s}$, when the tensions τ_1 and τ_2 start to increase and cable lengths l_1 and l_2 align with the blue curve. Finally, the velocity and length curves for cables $\mathcal{C}_5$ and $\mathcal{C}_6$ are the same during experiments E_2, E_4 and E_6, meaning that there was no need for slack correction after the change of six-cable configuration.

The AprilTag center-point trajectory in the image is visible in Fig. 7. The larger the initial cable slack, the larger the deviation from the straight-line trajectory. As the MP rapidly falls to a new cable configuration, it causes a sideways drift in the image trajectory. On the contrary, when TCA is used, the produced trajectories are very close to the desired straight lines. In conclusion, TCA improves the VS controller by reducing cable slack.

Eventually, cable slackness affects the accuracy of MP pose estimation, because the desired motion is not produced. In Fig. 8 the distance between the measured final MP pose and its estimation is shown for each experiment. Here, the rotational deviation is defined as the angle θ of the axis-angle $\theta\mathbf{u}$ representation of the rotation matrix ${}^{\widehat{p}}\mathbf{R}_p$ between the estimated and the actual MP pose. In E_1, E_2, E_4 and E_6 the estimation errors amount to 0.03 m and 2°. Thus, using TCA improves the MP pose estimation. It is significantly better in case of initial slack when compared to the classic controller. In E_5 the errors reach 9 cm and 5°. Given the short trajectory time of only 8 s, it can be concluded that large cable slack leads to fast deviation of the MP pose estimation. Moreover, the larger the initial cable slack, the larger the error in MP pose estimation.

C. Stability Analysis

This section deals with the stability analysis for the given experiments. The stability criterion $\mathbf{\Pi}$ is computed off-line as defined in (10) using the following recorded variables:

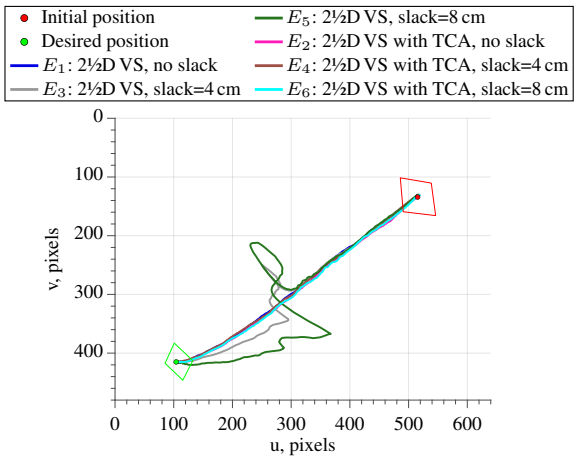

Fig. 7. AprilTag center-point trajectory in the image

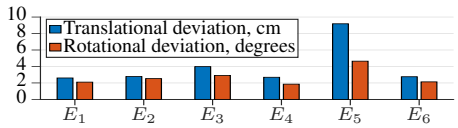

Fig. 8. Translational and rotational deviation of final MP pose estimation

- the same in the model and estimation: $\mathbf{s}$, $\mathbf{s}^*$, $\mathbf{L_s}$, A_i, B_i, ${}^p\mathbf{T}_c$, $\mathbf{A}_d$
- estimation: ${}^b\widehat{\mathbf{T}}_p$ as estimated by the controller
- model: ${}^b\mathbf{T}_p$ acquired by localizing an AprilTag on the MP via a static camera shown in Fig. 5.

Furthermore, cable slackness is also taken into account as described at the end of Section III.

Fig. 9 contains the results of stability analysis over time. Here, the boolean *Stable* is true if $\mathbf{\Pi} > \mathbf{0}$ and false otherwise. As expected, when no cable slack is added to the system, it remains stable throughout the trajectory no matter the controller, as shown in Fig. 9a. At one iteration one tension measurement goes below the threshold, however that does not make the system unstable, because there are still seven cables in tension. For E_3, shown in Fig. 9b in gray, at $t = 2.5$ s three cables become slack. Furthermore, at $t = 3.2$ s even four cables become slack. This leads to $\mathbf{\Pi} > \mathbf{0}$ no longer being true. Thus, when the MP is underactuated, it is no longer in static equilibrium and the stability of the system is not ensured. Hence, the static equilibrium of the MP and the stability of the system are linked. However, if TCA is used, it rapidly corrects the slack and the system remains stable all along the trajectory (see brown curve in Fig. 9b).

The behavior is analogous in E_5 and E_6, shown in Fig. 9c. Due to larger initial slack in E_5, the time period of underactuation is increased when compared to E_3. Similarly to E_4, in E_6 TCA successfully reduces slack, thus avoiding underactuation of the MP and loss of stability.

D. Tracking a mobile robot

The attached video contains a second experiment dealing with the MP following a mobile robot moving on a track over a prolonged time period. The velocity of the mobile robot is unknown, the VS controller is simply tasked to keep its AprilTag in the desired pose. To aid with MP pose estimation, a known tag is put on the track and the estimation is corrected every time it becomes visible. Despite this, the classic VS fails due to cable slack in lap 29 at $t < 10$ min. On the contrary, VS with TCA was perfectly functional after 700 laps, at $t > 180$ min.

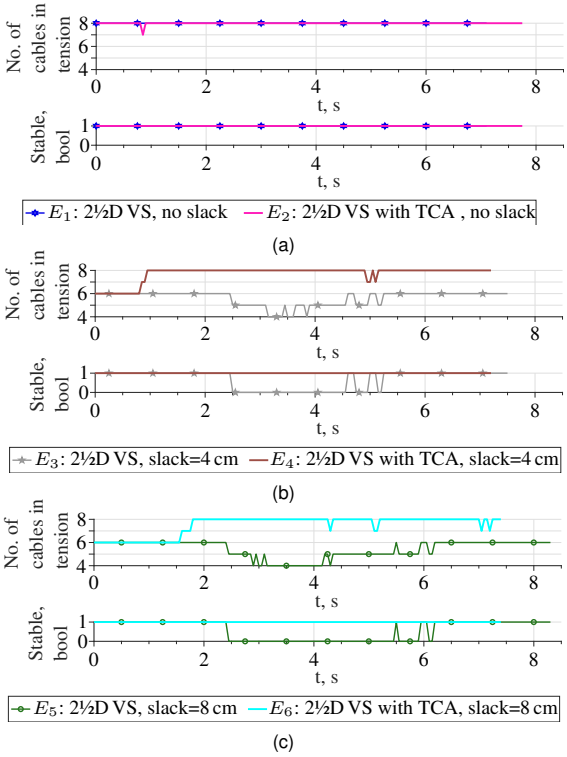

Fig. 9. The relation between the amount of cables in tension and system stability for: (a) no slack; (b) 4 cm slack; (c) 8 cm slack

V. Conclusions

This paper proposed the use of a tension feedback loop to deal with cable slackness. The algorithm is simple and improves the visual servoing controller. Indeed, the tension correction only occurs when cable slackness is detected and it is stopped as soon as the tension threshold is reached. The proposed algorithm is efficient in reducing cable slack and its rapidity depends on the tuning of the gain and the amount of slack on the cable.

Cable slack affects not only the CDPR responsiveness to control output, but also its stability. Indeed, when initial slack is large, the MP can become underactuated along the trajectory and that leads to the stability criterion being no longer ensured. In addition, the larger the cable slack, the larger the MP pose estimation error, when TCA is not used.

When cable slack is transferred between cables, the MP can sway uncontrollably, leading to sharp changes of the target trajectory in the image. As the cable slack increases, it becomes more likely that the target will leave the field of view, resulting in a task failure.

Future work includes the validation of the proposed controller on a fully-constrained CDPR and on a large-scale CDPR with elastic cables.

REFERENCES

[1] L. Gagliardini, S. Caro, M. Gouttefarde, A. Girin, "Discrete Reconfiguration Planning for Cable-Driven Parallel Robots", in *Mechanism and Machine Theory*, vol. 100, pp. 313–337, 2016.

[2] R. G. Roberts, T. Graham, T. Lippitt, "On the inverse kinematics, statics, and fault tolerance of cable-suspended robots", in *Journal of Robotic Systems*, vol. 215, no. 10, pp. 581–597, Oct. 1998.

[3] M. Gouttefarde, J. Lamaury, C. Reichert, T. Bruckmann, "A Versatile Tension Distribution Algorithm for 6-DOF Parallel Robots Driven by n+2 Cables", in *IEEE Transactions on Robotics*, vol. 31, no. 6, pp. 1444–1457, 2015.

[4] V. L. Schmidt, "Modeling Techniques and Reliable Real-Time Implementation of Kinematics for Cable-Driven Parallel Robots using Polymer Fiber Cables", Ph.D. dissertation, Fraunhofer Verlag, Stuttgart, Germany, 2017.

[5] E. Picard, S. Caro, F. Claveau, F. Plestan, "Pulleys and Force Sensors Influence on Payload Estimation of Cable-Driven Parallel Robots", in *IEEE Int. Conf. on Intelligent Robots and Systems*, Madrid, Spain, 2018, pp. 1429–1436.

[6] T. Dallej, M. Gouttefarde, N. Andreff, R. Dahmouche, P. Martinet, "Vision-based modeling and control of large-dimension cable-driven parallel robots", in *IEEE Int. Conf. on Intelligent Robots and Systems*, Vilamoura, Algarve, Portugal, 2012, pp. 1581–1586.

[7] T. Dallej, M. Gouttefarde, N. Andreff, P.-E. Hervé, P. Martinet, "Modeling and Vision-Based Control of Large-Dimension Cable-Driven Parallel Robots Using a Multiple-Camera Setup", in *Mechatronics*, vol. 61, pp. 20–36, 2019.

[8] R. Chellal, L. Cuvillon, E. Laroche, "A Kinematic Vision-Based Position Control of a 6-DoF Cable-Driven Parallel Robot", in *Cable-Driven Parallel Robots*, pp. 213–225, Springer, Cham, 2015.

[9] M. Zavatta, M. Chianura, A. Pott, M. Carricato, "A vision-based referencing procedure for cable-driven parallel manipulators", in *Journal of Mechanisms and Robotics*, vol. 12, no. 4, 2020.

[10] R. Ramadour, F. Chaumette, J.-P. Merlet, "Grasping Objects With a Cable-Driven Parallel Robot Designed for Transfer Operation by Visual Servoing", in *IEEE Int. Conf. on Robotics and Automation*, pp. 4463–4468, 2014.

[11] Z. Zake, F. Chaumette, N. Pedemonte, S. Caro, "Vision-Based Control and Stability Analysis of a Cable-Driven Parallel Robot", in *IEEE Robotics and Automation Letters*, vol. 4, no. 2, pp. 1029–1036, 2019.

[12] Z. Zake, F. Chaumette, N. Pedemonte, S. Caro, "Robust 2½D Visual Servoing of a Cable-Driven Parallel Robot Thanks to Trajectory Tracking", in *IEEE Robotics and Automation Letters*, vol. 5, no. 2, pp. 660–667, 2020.

[13] W. Kraus, V. Schmidt, P. Rajendra, A. Pott, "System identification and cable force control for a cable-driven parallel robot with industrial servo drives", in *IEEE Int. Conf. on Robotics and Automation*, pp. 5921–5926, 2014.

[14] A. Fortin-Côté, P. Cardou, C. Gosselin, "A tension distribution algorithm for cable-driven parallel robots operating beyond their wrench-feasible workspace", in *IEEE Int. Conf. on Control, Automation and Systems (ICCAS)*, pp. 68–73, 2016.

[15] E. Picard, S. Caro, F. Plestan, F. Claveau, "Stiffness Oriented Tension Distribution Algorithm for Cable-Driven Parallel Robots", in *The 17th International Symposium on Advances in Robot Kinematics*, Ljubljana, Slovenia, 2020, pp. 209–217.

[16] J. P. Merlet, "Simulation of discrete-time controlled cable-driven parallel robots on a trajectory", in *IEEE Transactions on Robotics*, vol. 33, no. 3, pp. 675–688, 2017.

[17] F. Chaumette, S. Hutchinson, P. Corke, "Visual Servoing", in *Handbook of Robotics*, 2nd edition, O. Khatib B. Siciliano (ed.), pp. 841–866, Springer, 2016.

[18] F. Chaumette, E. Malis, "2 1/2 D visual servoing: a possible solution to improve image-based and position-based visual servoings", in *IEEE Int. Conf. on Robotics and Automation*, pp. 630-635, 2000.

[19] V. Kyrki, D. Kragic, H. Christensen, "New shortest-path approaches to visual servoing", in *IEEE/RSJ Int. Conf on Intelligent Robots and Systems*, pp. 349–354, 2004.

[20] W. Khalil, E. Dombre, "Modeling, Identification and Control of Robots", Butterworth-Heinemann, 2004, pp. 13–29.

[21] A. Pott, "Cable-Driven Parallel Robots: Theory and Application", vol. 120, Springer, 2018, pp. 52–56.

[22] H. K. Khalil, Nonlinear systems, Macmillan publishing Co., 2nd ed., New York 1996.

[23] A. L. C. Ruiz, S. Caro, P. Cardou, F. Guay, "ARACHNIS: Analysis of Robots Actuated byCables with Handy and Neat Interface Software", in *Cable-Driven Parallel Robots*, pp. 293–305, Springer, Cham, 2015.

[24] E. Olson, "AprilTag: A robust and flexible visual fiducial system", in *IEEE Int. Conf. on Robotics and Automation*, pp. 3400–3407, 2011.

[25] É. Marchand, F. Spindler, F. Chaumette, "ViSP for visual servoing: a generic software platform with a wide class of robot control skills", in *IEEE Robotics & Automation Magazine*, vol. 12, no. 4, pp. 40–52, 2005.